Title

circCD2AP promotes epithelial mesenchymal transition and stemness in bladder cancer by regulating FOXQ1/USP21 axis.

Journal

iScience, 27(2)

Authors

Wang, Jinrong

Tan, Jing

Zhang, Yichuan

et al.

Publication Date

2024-02-16

DOI

10.1016/j.isci.2023.108447

Peer reviewed

iScience

CellPress
OPEN ACCESS

Article

circCD2AP promotes epithelial mesenchymal transition and stemness in bladder cancer by regulating FOXQ1/USP21 axis

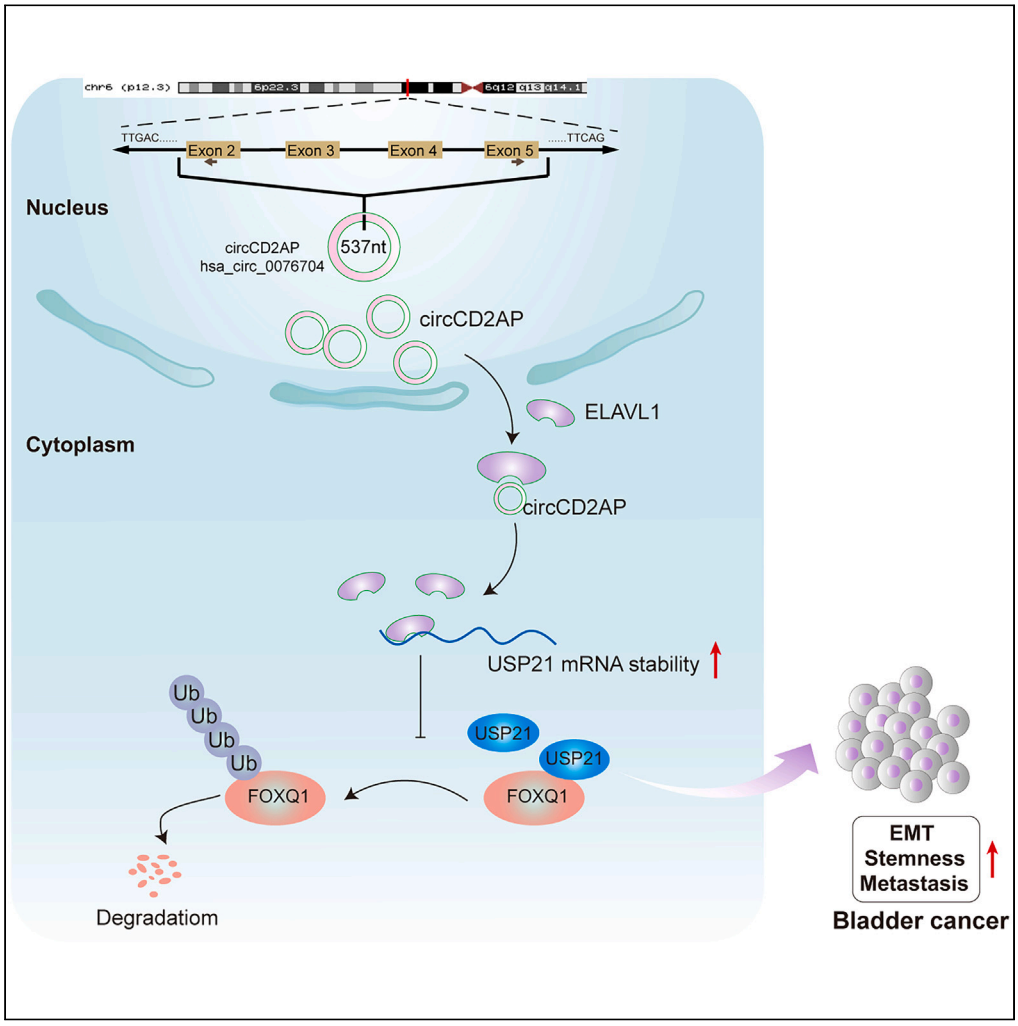

Jinrong Wang, Jing Tan, Yichuan Zhang, Lei Zhou, Yuan Liu

xy3yywjr@163.com

Highlights

High expression of circCD2AP is associated with poor prognosis in BC patients

circCD2AP enhances USP21 mRNA stability by interacting with ELAVL1

USP21 increases FOXQ1 levels by inhibiting its ubiquitination degradation

Knockdown of circCD2AP or USP21 inhibits EMT, stemness, and metastasis by FOXQ1

Wang et al., iScience 27, 108447
February 16, 2024
https://doi.org/10.1016/j.isci.2023.108447

iScience

CellPress
OPEN ACCESS

Article

circCD2AP promotes epithelial mesenchymal transition and stemness in bladder cancer by regulating FOXQ1/USP21 axis

Jinrong Wang,[1,2,*] Jing Tan,[1] Yichuan Zhang,[1] Lei Zhou,[1] and Yuan Liu[1]

SUMMARY

Bladder cancer (BC) is a prevalent and deadly disease. circCD2AP was suggested to be highly expressed in BC. However, the exact mechanism needs further investigation. In this study, circCD2AP was observed to be upregulated in BC and linked to poor prognosis in individuals. Functionally, circCD2AP or USP21 knockdown inhibited BC cell EMT and stemness both *in vitro* and *in vivo*. Mechanistically, circCD2AP interacted with ELAVL1 to enhance the stability of USP21 mRNA, which, in turn, inhibited the ubiquitination degradation of FOXQ1. Through rescue assay, USP21 or FOXQ1 knockdown was found to abolish the promoting effects of circCD2AP or USP21 overexpression on BC cell EMT and stemness. Overall, this study has unveiled the role of circCD2AP/ELAVL1/USP21/FOXQ1 axis in BC EMT and stemness regulation, offering insights into the mechanisms underlying BC progression, with potential implications for therapeutic strategies.

INTRODUCTION

Bladder cancer (BC) is a well-known urological malignancy prone to recurrence and distant metastasis, and it is often associated with a poor prognosis.[1] Platinum-based chemotherapy and new ICIs (cancer immunotherapy with immune checkpoint inhibitors) are the current standard therapy, providing unprecedented benefits to patients, and BC mortality has declined significantly in many countries over the past few decades.[2,3] However, the heterogeneity of BC has driven different clinical outcomes for BC patients.[4] Therefore, exploring early detection of biomarkers and markers of disease outcome as well as developing good surgical and medical therapies are important factors affecting the quality of life of BC patients.

In most cases, circular RNAs (circRNAs) are produced by a covalent linkage from 5′ to 3′ ends by back-splicing of linear RNA in animals.[5] Abnormal expression of many circRNAs is demonstrated in a variety of cancers, suggesting their vital effects in tumorigenesis and cancer progression.[6,7] In the study of BC, circ_0000658 was suggested to be upregulated in BC, and overexpression of circ_0000658 augmented oncogenic phenotypes and epithelial-mesenchymal transition (EMT) of cancer cells.[8] Circ_0030586 expression was decreased in BC tissues and cells, and overexpression of circ_0030586 suppressed cancer cell proliferation and stemness.[9] circCD2AP (circBase: hsa_circ_0076704) showed upregulation in BC tissues and cells, which have significant prognostic value by Kaplan Meier survival analysis and suggest becoming a prognostic marker and drug target for BC.[10] Nevertheless, the function and regulatory mechanisms of circCD2AP in BC are yet unknown. The publication also revealed the possibility of circCD2AP constructing a ceRNA network by binding to microRNA/target gene axis.[10] Indeed, a group of circRNAs exert biological functions by serving as protein decoys, scaffolds, and recruiters.[11] Herein, the data from bioinformatic analysis identified a potential binding relationship between circCD2AP and ELAV-like RNA-binding protein 1 (ELAVL1), an RNA-binding protein that has been reported to bind to HOXB-AS1 and then increase the stability of FUT4 mRNA in multiple myeloma.[12] We therefore speculated that the binding relationship between circCD2AP and ELAVL1 was also worth exploring.

De-ubiquitinating enzymes (DUBs) keep protein substrates stable by removing the ubiquitin molecules.[13,14] Ubiquitin-specific protease 21 (USP21), as an effective DUB, has been found to participate in the malignant processes of multiple tumors. For instance, several publications have discussed the role of USP1 on regulating EMT process and stemness of cancer cells. Furthermore, USP21 was highly expressed in BC and promote EMT *in vitro* through its DUB activity.[15] USP21 stimulated pancreatic cancer cell stemness through activating the Wnt pathway.[16] Bioinformatics analysis revealed that ELAVL1 bound to USP21, and ELAVL1 positively correlates with USP21 in BC.

Forkhead box Q1 (FOXQ1) is a member of the forkhead box family of transcription factors, composed of 44 members in humans, all of which share a common DNA-binding domain (DBD).[17] We previously revealed the promoting function of FOXQ1 on BC cell proliferation and metastasis.[18] Several other studies have suggested that FOXQ1 was a key factor in the regulation of tumor stemness and EMT. For

[1]Department of Urology, The Third Xiangya Hospital of Central South University, Changsha 410013, Hunan Province, China
[2]Lead contact
*Correspondence: xy3yywjr@163.com
https://doi.org/10.1016/j.isci.2023.108447

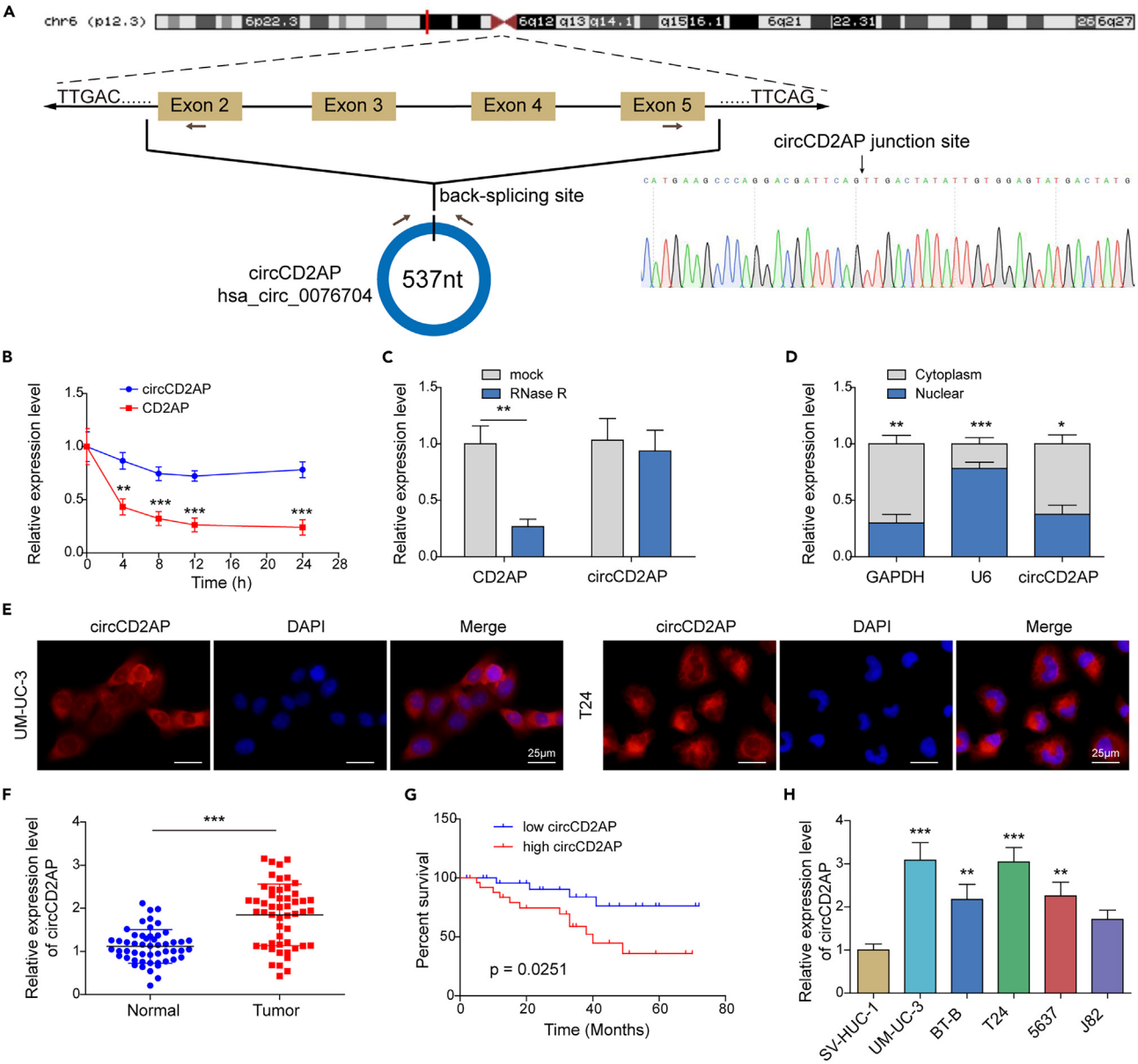

Figure 1. The upregulation of circCD2AP was observed and linked to poor prognosis in BC patients

(A) Sanger sequencing validation for circCD2AP.

(B and C) Act-D and RNase treatment analyzed circCD2AP stability.

(D and E) The location of circCD2AP was identified by qRT-PCR and FISH. Scale bar: 25 μm.

(F) circCD2AP expression in 52 paired tumor tissues and matched adjacent normal tissues was measured by qRT-PCR.

(G) Kaplan-Meier survival curves in BC individuals based on circCD2AP levels.

(H) qRT-PCR analysis of circCD2AP in cancer cell lines (5637, T24, UM-UC-3, BT-B, and J82) and human normal bladder epithelial cells (SV-HUC-1). Mean ± SD, n = 3, *p < 0.05, **p < 0.01, ***p < 0.001. Statistical analysis was carried out by a Student's t test or a one-way ANOVA.

instance, miR-4319 repressed hepatocellular carcinoma cell proliferation and EMT and reduced cancer stemness *in vitro* via interacting with FOXQ1.[19] FOXQ1 knockdown induced BC cells to acquire an epithelial cobblestone phenotype, significantly reducing cell motility and subsequent invasiveness.[20] On the other hand, USP21 was found to deubiquitinate and stabilize FOXM1 protein,[21] which is in the same family as FOXQ1, so is the FOXQ1 protein also regulated by USP21 ubiquitination? For all above-mentioned reasons, we proposed the hypothesis that circCD2AP promoted USP21 stability by binding to ELAVL1; subsequently, the upregulation of USP21 inhibits FOXQ1 ubiquitination degradation, thereby promoting BC EMT and stemness.

Table 1. Correlation of the expression levels of circCD2AP with the clinicopathological characteristics of bladder cancer patients

		circCD2AP expression		
Clinical parameters	Cases (n)	High (n)	Low (n)	p value
Age				0.397
<60 years	21	9	12	
≥60 years	31	17	14	
Gender				0.532
Male	38	20	18	
Female	14	6	8	
Tumor size (cm)				0.052
<3	27	10	17	
≥3	25	16	9	
Histological grade				0.032*
High	37	22	15	
Low	15	4	11	
T stage				0.048*
Ta-T1	21	7	14	
T2-T4	31	19	12	
Lymph node metastasis				0.026*
N0	28	10	18	
N1-3	24	16	8	
Distant metastasis				0.044*
M0	33	13	20	
M1	19	13	6	

*$p < 0.05$.

RESULTS

The upregulation of circCD2AP was observed and linked to poor prognosis in BC patients

circCD2AP (circBase: hsa_circ_0076704) arose from exons 2 to 5 of the CD2AP gene, and its spliced mature sequence length is 537 nt. The head-to-tail splicing was verified through Sanger sequencing (Figure 1A). circCD2AP had a longer half-life than CD2AP gene and can be resistant to the degradation by RNase R, indicating that circCD2AP was in a form of stable ring structure (Figures 1B and 1C). Moreover, circCD2AP was distributed in both nucleus and cytoplasm, while mainly locating in the cytoplasm (Figures 1D and 1E). Compared with normal tissues, higher circCD2AP levels were observed in BC tissues (Figure 1F), which linked to a poor prognosis in individuals (Figure 1G). Furthermore, elevated circCD2AP levels showed a robust association with the TNM stage and histological grade in BC individuals, while being unrelated to other clinical features, such as age, gender, and tumor size (Table 1). Besides, circCD2AP was upregulated in BC cells (5637, T24, UM-UC-3, BT-B, and J82), and was most increased in UM-UC-3 and T24 cells (Figure 1H), prompting us to select these two cells for subsequent assays. In conclusion, abnormal expression of circCD2AP might be a key factor affecting overall survival of BC patients.

Knockdown of circCD2AP inhibited the EMT and stemness of BC cells

Next, we investigated the biological function of circCD2AP, focusing on EMT and stemness. The plasmids shcircCD2AP#1 and shcircCD2AP#2 were successfully transfected into cells, which decreased circCD2AP expression and had no significant effect on linear CD2AP expression (Figures 2A and 2B). To exclude the possible off-target effects of the shRNA system, a rescue experiment was performed with an shRNA-resistant form of the circCD2AP (with target site mutated), and qRT-PCR showed that circCD2AP levels increased back after the transduction of shcircCD2AP-Res (Figure 2A). Subsequently, circCD2AP silencing inhibited BC cell viability (Figure 2C). Stemness gene levels, the tumor-sphere-forming ability, and the proportion of $CD133^+$ cells were detected to assess the ability of circCD2AP to maintain the stemness of BC cells. OCT4, Nanog, Sox2, ALDH1A1, and CD44v6 levels were repressed by silencing circCD2AP (Figures 2D–2H). The decreases in the numbers of tumor spheres were observed after knocking down circCD2AP (Figure 2I). The percentage of $CD133^+$ cell subfraction was significantly reduced by silencing circCD2AP (Figure 2K). Additionally, knockdown of circCD2AP regulated a morphologic change indicative of EMT (Figure 2J). Moreover, cell migration and EMT-related markers expression were analyzed after knocking down circCD2AP. Knockdown of circCD2AP inhibited BC cell migration (Figure 2L) and reduced Twist1, N-cadherin, and vimentin expression, while increasing E-cadherin

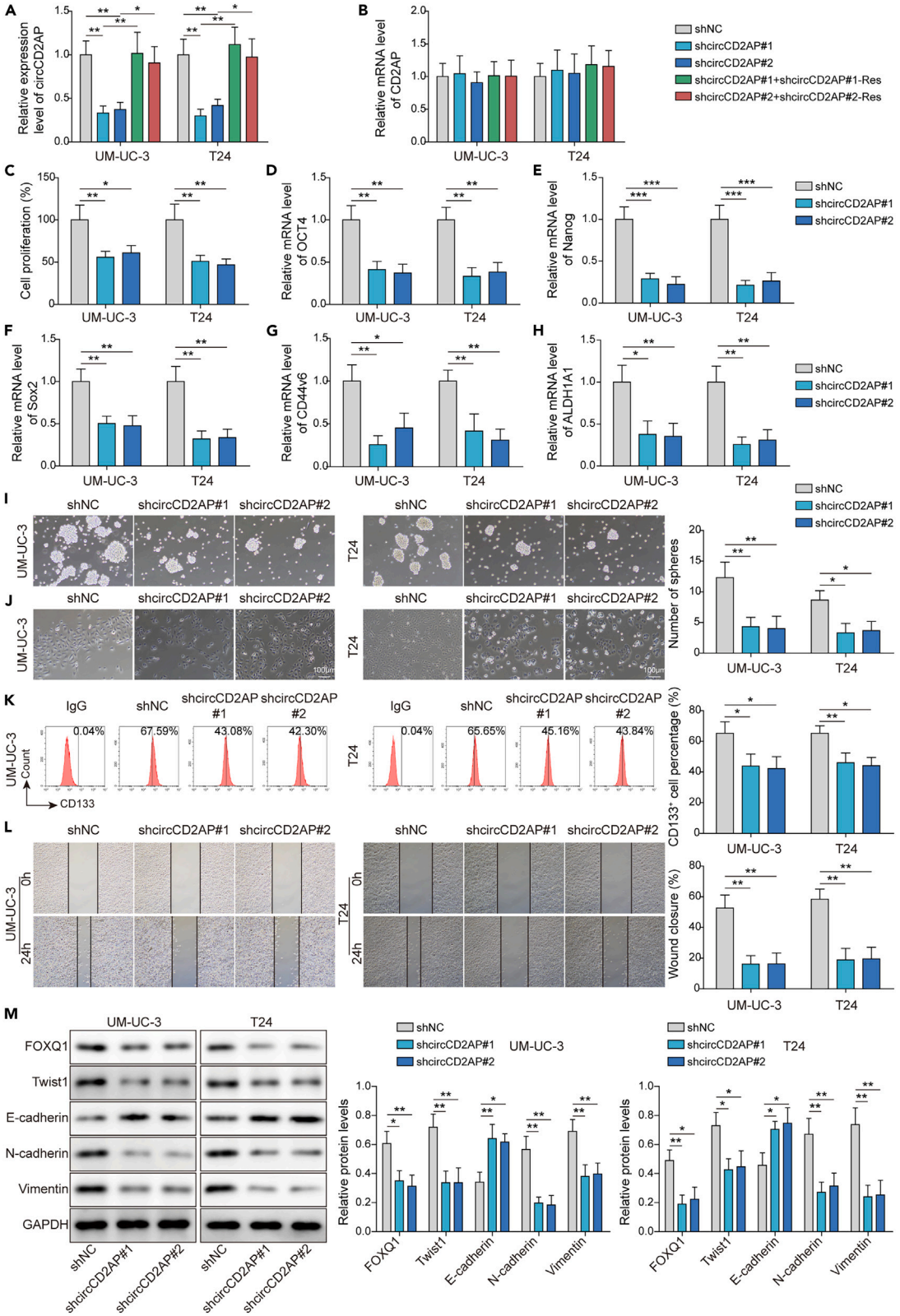
A
Relative expression level of circCD2AP
UM-UC-3
T24
B
Relative mRNA level of CD2AP
shNC
shcircCD2AP#1
shcircCD2AP#2
shcircCD2AP#1+shcircCD2AP#1-Res
shcircCD2AP#2+shcircCD2AP#2-Res
C
Cell proliferation (%)
D
Relative mRNA level of OCT4
E
Relative mRNA level of Nanog
F
Relative mRNA level of Sox2
G
Relative mRNA level of CD44v6
H
Relative mRNA level of ALDH1A1
I
shNC
shcircCD2AP#1
shcircCD2AP#2
UM-UC-3
T24
Number of spheres
J
K
IgG
shNC
shcircCD2AP #1
shcircCD2AP #2
0.04%
67.59%
43.08%
42.30%
0.04%
65.65%
45.16%
43.84%
Count
CD133
CD133+ cell percentage (%)
L
0h
24h
Wound closure (%)
M
FOXQ1
Twist1
E-cadherin
N-cadherin
Vimentin
GAPDH
Relative protein levels

Figure 2. Knockdown of circCD2AP inhibited the EMT and stemness of BC cells

(A and B) qRT-PCR analysis of circCD2AP and CD2AP mRNA in UM-UC-3 and T24 cells after transfecting with shcircCD2AP#1 or shcircCD2AP#2.

(C) Cell viability was determined through CCK-8 after silencing circCD2AP.

(D–H) qRT-PCR analysis of stemness genes (OCT4, Nanog, Sox2, ALDH1A1, and CD44v6).

(I) Sphere-formation assay determined cell stemness after knocking down circCD2AP.

(J) The observation of morphological changes of cells silenced circCD2AP. Scale bar: 100 μm.

(K) $CD133^+$ cell percentage was analyzed in cells silenced circCD2AP by flow cytometry.

(L) Cell migration was detected via wound-healing assay after silencing circCD2AP.

(M) The expression of FOXQ1 and EMT-related markers (Twist1, N-cadherin, E-cadherin, and vimentin) in cancer cells was measured by western blotting after knocking down circCD2AP. GAPDH used as control. Mean ± SD, *$p < 0.05$, **$p < 0.01$, ***$p < 0.001$. Statistical analysis was carried out by a one-way ANOVA.

levels (Figure 2M). Besides, FOXQ1 expression was inhibited by silencing circCD2AP (Figure 2M). Taken together, circCD2AP was involved in the processes of EMT and stemness of BC cells.

CircCD2AP upregulated USP21 through enhancing the stability of USP21 by binding to ELAVL1

USP21 has suggested to participate in the proliferation and metastasis of BC cells.[15] By analyzing the data obtained from UALCAN database (Database: https://ualcan.path.uab.edu/analysis.html) and the clinical sample, we demonstrated that USP21 was markedly upregulated in BC tissues (Figures S3A and 3A). Interestingly, its levels were positively correlated with circCD2AP levels both in tumor tissues and BC cell lines (Figures 3B and S3C). The mRNA and protein levels of USP21 levels were significantly increased in BC cell lines (Figures 3C and 3D). Moreover, USP21 mRNA and protein levels were inhibited in cells transfected with shcircCD2AP#1 or shcircCD2AP#2 (Figures 3E and 3F), indicating the potential regulatory relationship between circCD2AP and USP21. Through RNA pull-down and RIP assays, we found that circCD2AP probe could enrich ELAVL1 in UM-UC-3 and T24 cells (Figure 3G), and circCD2AP and USP21 could be enriched by ELAVL1 antibody (Figures 3H and 3I), confirming the targeting relationship between them. Moreover, knockdown of circCD2AP inhibited the enrichment of USP21 induced by ELAVL1 antibody (Figure 3J). Act-D was added into cells silenced circCD2AP to assess the stability of USP21 mRNA. As shown in Figure 3K, knockdown of circCD2AP repressed the stability of USP21 mRNA. Furthermore, knockdown of ELAVL1 also reduced the stability of USP21 mRNA in UM-UC-3 and T24 cells (Figure 3L). Therefore, circCD2AP enhanced the stability of USP21 and increased its expression by interacting with ELAVL1.

circCD2AP promoted EMT and stemness of BC cells through upregulating USP21

Next, we designed and performed two sets of rescue assays to investigate the function of circCD2AP/USP21 axis on BC cell EMT and stemness. The USP21 plasmids were transfected into UM-UC-3 and T24 cells to overexpress USP21 expression (Figures 4A and 4B). Overexpression of USP21 was observed to block the inhibitory effects of circCD2AP knockdown on BC cell viability (Figure 4C). Moreover, the decreased OCT4, Nanog, Sox2, and ALDH1A1 levels, repressed tumor-sphere-forming ability, and reduced percentage of $CD133^+$ cells in cells silenced circCD2AP were abolished after overexpressing USP21 (Figures 4D–4I), suggesting that USP21 overexpression reversed the inhibition of BC cell stemness caused by silencing circCD2AP. USP21 overexpression also blocked the inhibitory effect of circCD2AP knockdown on cell migration (Figure 4J). The downregulation of Twist1, N-cadherin, and vimentin and the upregulation of E-cadherin in cells silenced circCD2AP were reversed by overexpressing USP21 (Figure 4K), indicating that circCD2AP-knockdown-induced inhibition of cell EMT was abolished by USP21 overexpression. Besides, the decreased FOXQ1 levels in cells silenced circCD2AP were recovered after overexpressing USP21 (Figure 4K). These findings suggested that USP21 overexpression reversed the inhibiting effects of circCD2AP knockdown on the EMT and stemness of BC cells.

Subsequently, USP21 levels were inhibited by transfecting with shUSP21, and circCD2AP expression was increased by transfecting with circCD2AP (Figures S1A–S1C). Knockdown of USP21 inhibited the proliferation of BC cells, whereas overexpression of circCD2AP reversed this change (Figure S1D). Furthermore, knockdown of USP21 downregulated OCT4, Nanog, Sox2, and ALDH1A1, suppressed the tumor-sphere-forming ability, and reduced the percentage of $CD133^+$ cells, whereas overexpression of circCD2AP blocked these inhibiting effects (Figures S1E–S1J). As expected, the migration ability and EMT of BC cells were repressed by silencing USP21, whereas overexpression of circCD2AP abrogated these changes (Figures S1K and S1L). Furthermore, circCD2AP overexpression could increase USP21 levels in cells silenced USP21, indicating that circCD2AP overexpression can rescue USP21 knockdown. This could be attributed to cirCD2AP's ability to enhance USP21 expression by stabilizing it (Figure S1L). In conclusion, circCD2AP promoted the EMT and stemness of BC cells by upregulating USP21.

USP21 upregulated FOXQ1 by inhibiting its ubiquitination degradation

Although we observed no significant difference in FOXQ1 expression in tumor tissues compared with normal tissue by using TCGA database (Figure S3B) (the difference in FOXQ1 expression may not have been detected because of the small number of cases in the normal group in the database [only 19 cases]), previous study demonstrated the upregulation of FOXQ1 in BC and its promoting roles on cell growth and metastasis.[18] Besides, FOXQ1 levels were regulated by circCD2AP or USP21 (Figures 2J, 4K and S1L). These evidences indicated that FOXQ1 was a factor worth exploring in circCD2AP/USP21-axis-related pathway. Here, we observed that the downregulation of FOXQ1 in UM-UC-3 and T24 cells caused by knockdown of circCD2AP or USP21 was inhibited after treating with proteasome inhibitor MG132

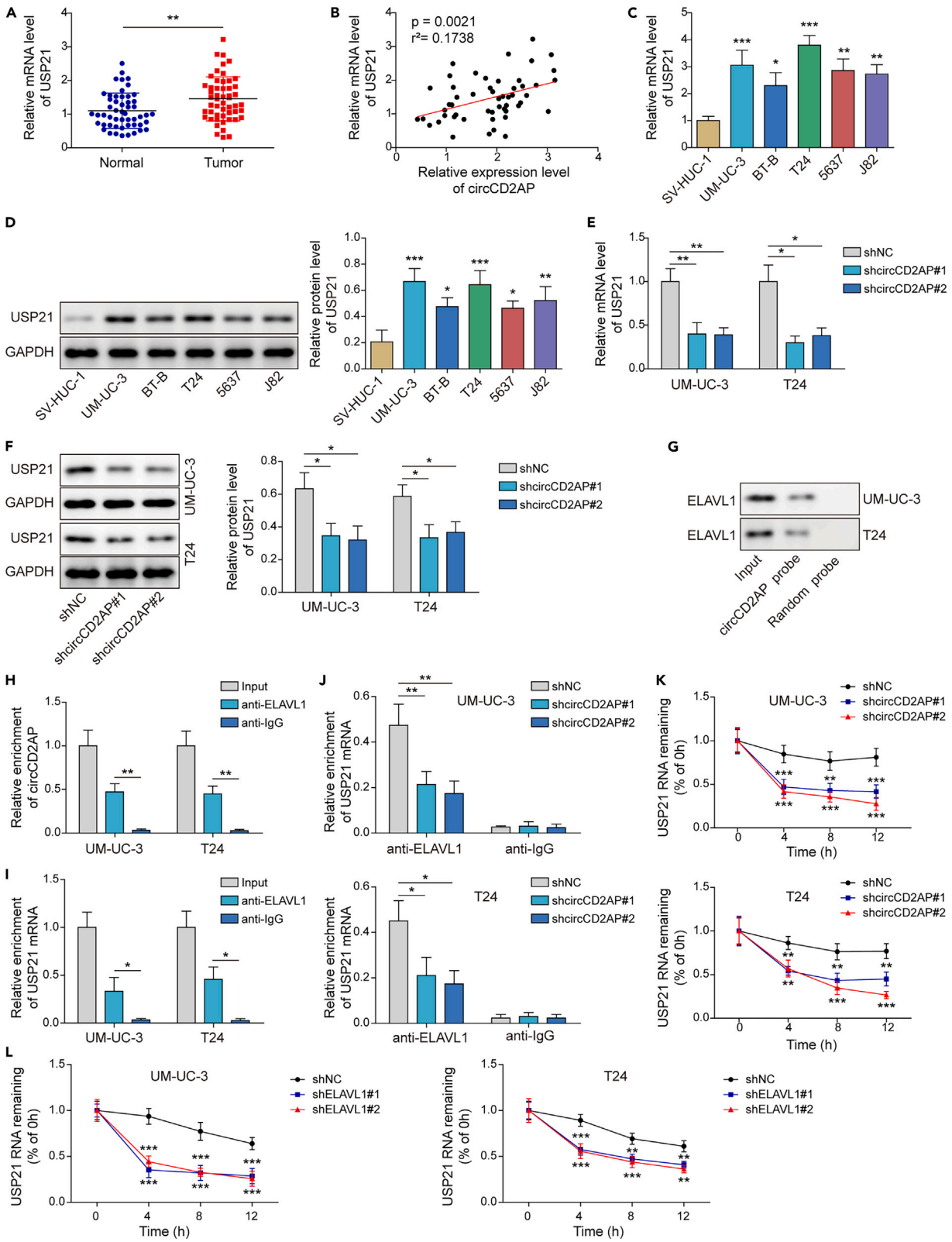
A
Relative mRNA level of USP21
Normal
Tumor
B
p = 0.0021
r²= 0.1738
Relative mRNA level of USP21
Relative expression level of circCD2AP
C
Relative mRNA level of USP21
SV-HUC-1
UM-UC-3
BT-B
T24
5637
J82
D
USP21
GAPDH
Relative protein level of USP21
E
Relative mRNA level of USP21
shNC
shcircCD2AP#1
shcircCD2AP#2
F
USP21
GAPDH
UM-UC-3
T24
shNC
shcircCD2AP#1
shcircCD2AP#2
Relative protein level of USP21
G
ELAVL1
Input
circCD2AP probe
Random probe
H
Input
anti-ELAVL1
anti-IgG
Relative enrichment of circCD2AP
I
Relative enrichment of USP21 mRNA
J
Relative enrichment of USP21 mRNA
anti-ELAVL1
anti-IgG
K
USP21 RNA remaining (% of 0h)
Time (h)
L
shELAVL1#1
shELAVL1#2

Figure 3. CircCD2AP upregulated USP21 through enhancing the stability of USP21 by binding to ELAVL1

(A) qRT-PCR analysis of USP21 in 52 paired BC tissue and matched adjacent normal tissue.

(B) Correlation analysis of circCD2AP and USP21.

(C and D) qRT-PCR and western blotting analysis of USP21 in BC and SV-HUC-1 cells. GAPDH used as control.

(E and F) USP21 levels in UM-UC-3 and T24 cells were detected after silencing circCD2AP.

(G) RNA pull-down analyzed the binding properties between circCD2AP and ELAVL1.

(H and I) RIP assay performed to evaluate the interactions between ELAVL1 and circCD2AP or USP21.

(J) RIP assay detected the binding relationship between ELAVL1 and USP21 in cells silenced circCD2AP.

(K and L) The stability of USP21 mRNA was analyzed by act-D treatment in cells silenced circCD2AP or ELAVL1. Mean ± SD, n = 3, *p < 0.05, **p < 0.01, ***p < 0.001. Statistical analysis was carried out by a one-way ANOVA.

(Figure 5A). As shown in Figure 5B, FOXQ1 was enriched by USP21 antibody, suggesting the targeted relationship between them. Subsequently, we found that knockdown of circCD2AP or USP21 increased the ubiquitination levels of FOXQ1 (Figure 5C). Next, *de novo* protein synthesis was blocked by cycloheximide (CHX) treatment, followed by measuring FOXQ1 protein levels at the indicated intervals. The results showed that circCD2AP or USP21 depletion accelerated FOXQ1 protein turnover in both UM-UC-3 and T24 cells (Figure 5D). These findings suggested that USP21 interacted with FOXQ1 and the downregulation of circCD2AP or USP21 accelerated FOXQ1 degradation.

circCD2AP promoted EMT and stemness of BC cells through regulating USP21/FOXQ1 axis

Next, we began to further investigate the biological function of circCD2AP/USP21/FOXQ1 axis on BC cell EMT and stemness through performing rescue assays. FOXQ1 plasmids were successfully transfected into UM-UC-3 and T24 cells to increase FOXQ1 expression (Figures 6A and 6B). Subsequently, we observed that knockdown of circCD2AP or USP21 could repress BC cell proliferation, whereas FOXQ1 overexpression blocked this effect (Figure 6C). Knockdown of circCD2AP or USP21 deceased the expression OCT4, Nanog, Sox2, and ALDH1A1 (Figures 6D–6G), suppressed tumor-sphere-forming ability (Figure 6H), and reduced the percentage of $CD133^+$ cells (Figure 6I), suggesting their inhibitory effects on BC cell stemness, whereas overexpression of FOXQ1 blocked these effects (Figures 6D–6I). Furthermore, the repressed migratory capacity of BC cells caused by silencing circCD2AP or USP21 was recovered after overexpressing FOXQ1 (Figure 6J). Overexpression of FOXQ1 abolished the inhibitory effect of circCD2AP or USP21 knockdown on cell EMT (Figure 6K). Therefore, overexpression of FOXQ1 blocked the inhibitory effects of circCD2AP or USP21 knockdown on EMT and stemness of BC cells.

To further strengthen the aforementioned conclusion, we conducted another set of rescue assays. shFOXQ1 transfection successfully downregulated FOXQ1 (Figures S2A and S2B). Knockdown of FOXQ1 repressed the proliferation of BC cells, whereas overexpression of circCD2AP or USP21 could block this inhibiting effect (Figure S2C). Moreover, knockdown of FOXQ1 showed inhibiting effects on the expression of OCT4, Nanog, Sox2, and ALDH1A1 (Figures S2D–S2G), tumor-sphere-forming ability (Figure S2H), and percentage of $CD133^+$ cells (Figure S2I), suggesting that FOXQ1 knockdown could suppress stemness of BC cells, whereas overexpression of circCD2AP or USP21 blocked these inhibiting effects (Figures S2D–S2I). The inhibition on BC cell migration and EMT caused by FOXQ1 knockdown was also abolished after overexpressing circCD2AP or USP21 (Figures S2J and S2K). Additionally, simultaneous overexpression of circCD2AP or USP21 significantly increased FOXQ1 levels in cells silenced FOXQ1, reaching levels equivalent to the shNC+Vector group, which suggested that overexpression of circCD2AP or USP21 could rescue the downregulation of FOXQ1 by promoting FOXQ1 expression (Figure S2K). Taken together, knockdown of FOXQ1 blocked the function of circCD2AP or USP21 overexpression on EMT and stemness of BC cells.

Knockdown of circCD2AP inhibited tumor formation and lung metastasis through suppression of USP21-mediated FOXQ1 signaling in nude mice

The *in vivo* experiments were performed to further verify the biological function of circCD2AP/USP21/FOXQ1 pathway. Nude mice were injected with T24 cells that stably expressed shcircCD2AP or shUSP21. circCD2AP or USP21 silencing significantly suppressed mice tumor growth (Figures 7A–7C). Knockdown of circCD2AP or USP21 inhibited the expression of USP21, OCT4, Nanog, Sox2, and ALDH1A1 in tumor tissues (Figures 7D–7H), suggesting the inhibiting effects of circCD2AP or USP21 knockdown on cancer cell stemness. Moreover, knockdown of circCD2AP or USP21 repressed FOXQ1, Twist1, N-cadherin, and vimentin levels in tumor tissues, while facilitating E-cadherin levels (Figure 7I), indicating their inhibiting effects on EMT process. The results from IHC analysis indicated that circCD2AP or USP21 knockdown suppressed Ki-67, CD133, and FOXQ1 expression in tumor tissues (Figure 7J). We also analyzed the lung metastasis. As shown in Figures 7K and 7L, knockdown of circCD2AP or USP21 reduced the lung metastatic nodules. These findings suggested that circCD2AP regulated tumor formation and lung metastasis through USP21/FOXQ1 axis.

DISCUSSION

BC has been identified as one of the most associated with mutation tumors in humans, with mutation rates second only to lung and skin cancer, and causing a huge burden to society and patients.[22,23] Despite the fact that a number of innovative innovations have been developed in recent years to help with the diagnosis and treatment of BC,[24] the incidence and mortality rates of BC have not improved significantly, and the prognosis of patients remains poor. These limitations prompted us to develop more efficiency treatment targets to improve clinical outcomes for BC patients. In this study, circCD2AP was overexpressed in BC tissues and cells. Increased circCD2AP enhanced the stability of USP21 mRNA by binding with ELAVL1, and then the upregulation of USP21 facilitated BC cell EMT and stemness by inhibiting the ubiquitination degradation of FOXQ1.

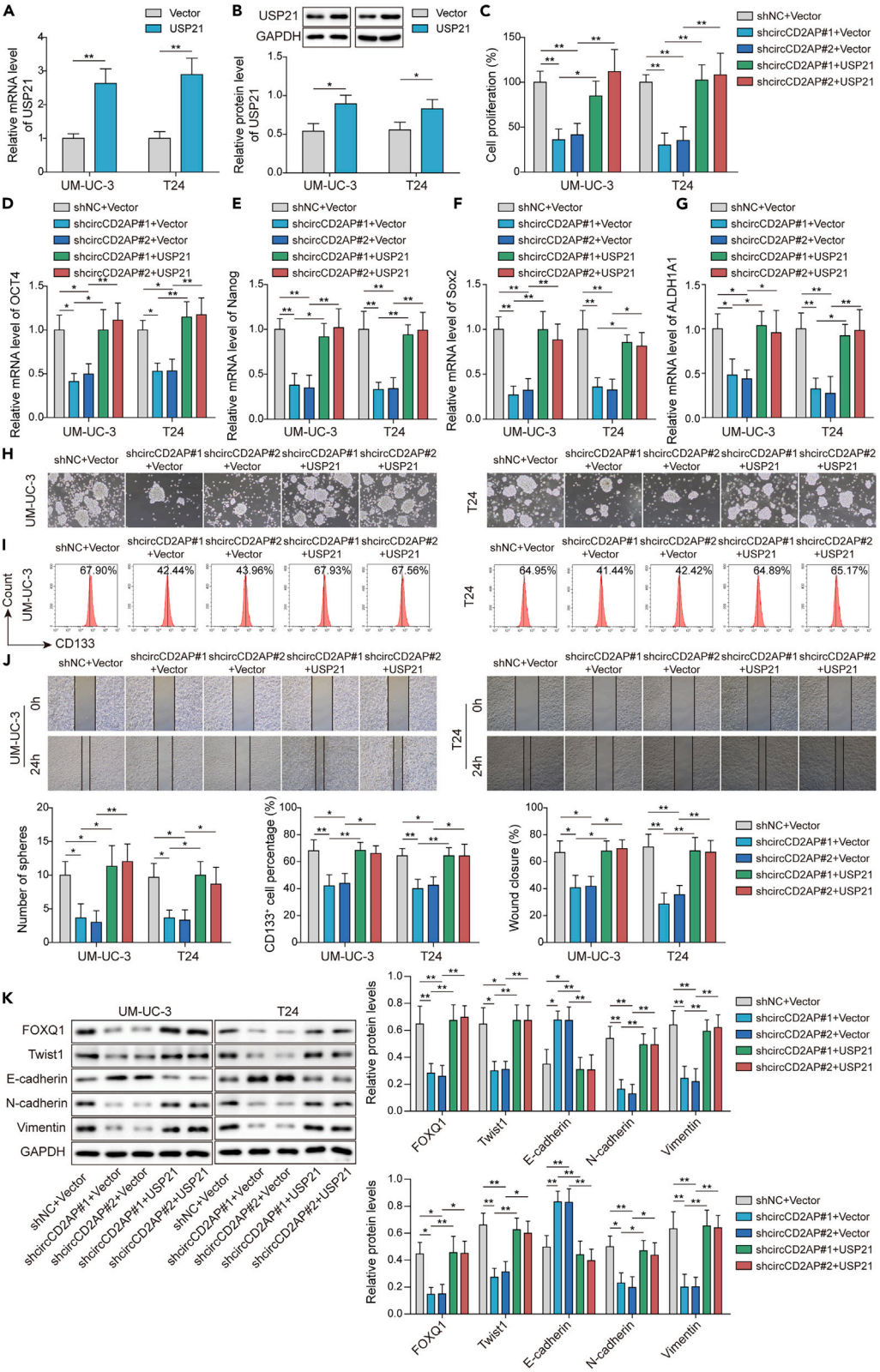
A
Vector
USP21
Relative mRNA level of USP21
UM-UC-3
T24
B
USP21
GAPDH
Vector
USP21
Relative protein level of USP21
UM-UC-3
T24
C
shNC+Vector
shcircCD2AP#1+Vector
shcircCD2AP#2+Vector
shcircCD2AP#1+USP21
shcircCD2AP#2+USP21
Cell proliferation (%)
UM-UC-3
T24
D
Relative mRNA level of OCT4
E
Relative mRNA level of Nanog
F
Relative mRNA level of Sox2
G
Relative mRNA level of ALDH1A1
H
UM-UC-3
T24
I
Count
CD133
67.90%
42.44%
43.96%
67.93%
67.56%
64.95%
41.44%
42.42%
64.89%
65.17%
J
0h
24h
Number of spheres
CD133+ cell percentage (%)
Wound closure (%)
K
FOXQ1
Twist1
E-cadherin
N-cadherin
Vimentin
GAPDH
Relative protein levels

Figure 4. circCD2AP promoted EMT and stemness of BC cells through upregulating USP21

(A and B) Analysis of overexpression efficiency of USP21 plasmid in UM-UC-3 and T24 cells. GAPDH used as control.

(C) The viability of cells co-transfected with shcircCD2AP#1+USP21 or shcircCD2AP#2+USP21 was measured by CCK-8.

(D–G) The expression of OCT4, Nanog, Sox2, and ALDH1A1 in UM-UC-3 and T24 cells was evaluated by qRT-PCR after simultaneously silencing circCD2AP and overexpressing USP21.

(H) Cancer cell stemness was evaluated by sphere-formation assay after simultaneously silencing circCD2AP and overexpressing USP21.

(I) The percentage of $CD133^+$ cells were analyzed in cells co-transfected with shcircCD2AP#1+USP21 or shcircCD2AP#2+USP21 by flow cytometry.

(J) The migration of cells co-transfected with shcircCD2AP#1+USP21 or shcircCD2AP#2+USP21 was measured by wound-healing assay.

(K) Western blotting analysis of FOXQ1, Twist1, N-cadherin, E-cadherin, and vimentin after simultaneously silencing circCD2AP and overexpressing USP21. GAPDH used as control. Mean ± SD, *$p < 0.05$, n = 3, **$p < 0.01$, ***$p < 0.001$. Statistical analysis was carried out by a Student's t test or a one-way ANOVA.

circRNAs are abundant in eukaryotes, expressed abnormally in malignant tumors, and more importantly, can serve as effective biomarkers due to their high stability.[25,26] circRNAs have been shown to drive BC carcinogenesis through multiple mechanisms, including those that promote cell proliferation and metastasis, enhance EMT, maintain stemness, and make it resistant to chemotherapy.[27,28] For instance, hsa_circ_0008532 was upregulated in BC and interacted with miR-155-5p and miR-330-5p to enhance MTGR1 levels, thereby inhibiting the activity of downstream NOTCH pathway,[29] the deletion of which has been shown to promote EMT in BC cells.[30] Hsa_circ_0068307 silencing suppressed cell migration and proliferation in T24 and UM-UC-3 cells and reversed the stem-cell-like properties of BC through regulating miR-147/c-Myc axis.[31] Here, we focused on circCD2AP as it was previously shown to be aberrantly expressed in BC.[10] We identified that circCD2AP had high stability and showed high expression in BC. Functionally, circCD2AP silencing was suggested to inhibit EMT and stemness of BC cells. Therefore, the specific mechanism of its regulation of bladder carcinogenesis deserved further investigation.

circRNAs are involved in tumorigenesis mainly through the following mechanisms: acting as a "miRNA sponge," binding to proteins, regulating mRNA stability, transcriptional regulation, and translation of proteins.[32] In BC, most researchers have reported the functions of circRNAs as miRNA sponges.[33–35] In our study, we validated that circCD2AP acted as an oncogene not via the ceRNA mechanism, but through interacting with ELAVL1 protein. In addition, ELAVL1 antibody was found to enrich not only circCD2AP but also USP21. Previous studies demonstrated that ELAVL1 was responsible for stabilizing and translating many target mRNAs.[12,36] Besides, circRNAs can regulate the stabilization and translation of mRNAs by binding with ELAVL1.[37] Consistently, our findings suggested that circCD2AP enhanced the stability of USP21 and increased its expression by interacting with ELAVL1. USP21 protein is highly conserved between humans and mice (97% similarity)[38] and exhibit oncogenic functions in multiple tumor types. Guo et al. suggested that USP21 regulated MAPK1 through interacting with GATA3, thus regulating the tumor growth and cell stemness of gastric cancer.[39] In the study of BC, USP21 was found to be highly expressed and promotes EMT *in vitro* through its DUB activity.[15] Herein, knockdown of USP21 repressed BC cell EMT and stemness *in vitro* and *in vivo* and abolished the promoting effects of circCD2AP overexpression on cancer cell EMT and stemness. Furthermore, FOXQ1 was lowered by circCD2AP or USP21, indicating a possible regulatory network between circCD2AP, USP21, and FOXQ1.

USP21 deubiquitinates many cytoplasmic and nuclear substrates.[40,41] Here, our findings proved that USP21 deubiquitinated FOXQ1 and thus stabilized it. Moreover, knockdown of circCD2AP or USP21 could accelerate FOXQ1 degradation, suggesting that circCD2AP inhibited the degradation of FOXQ1 by regulating USP21. Based on our previous study, FOXQ1, which acts as an oncogene, facilitated BC cell viability and metastasis.[18] Indeed, several other reports have revealed the important roles of FOXQ1 in cancer cell proliferation, motility, EMT, and stemness.[42–44] For example, miR-4319 repressed cell proliferation, accelerated apoptosis, inhibited EMT, and prevented cancer stemness in hepatocellular carcinoma cells by targeting FOXQ1.[19] Hence, we speculated that FOXQ1 was a key participant in the mechanism of circCD2AP/USP21 pathway in BC progression. Our results from rescue assays suggested that FOXQ1 overexpression abolished the inhibitory effects of circCD2AP or USP21 knockdown on BC cell EMT and stemness. Previous studies have focused on circRNA as ceRNA to regulate FOXQ1-related pathways involved in cancer development and progression,[45,46] whereas we illustrated for the first time how circCD2AP facilitated FOXQ1 expression via the regulation of deubiquitinating enzyme, USP21, thereby promoting bladder cancer EMT and cell stemness.

In conclusion, circCD2AP inhibited the ubiquitination degradation of the pro-oncogenic factor FOXQ1 by enhancing the stability of USP21 through interacting with ELAVL1, and ultimately promoted BC cell EMT and stemness, highlighting the circCD2AP/USP21/FOXQ1 cascade as a potential therapeutic target for conquering BC.

Limitations of the study

One limitation of our study is that we opted for cell lines with diverse mutational properties for our experiments. The specific BC cell lines were chosen mainly due to their availability in our laboratory. However, utilizing cell lines with mutations in functionally similar targets might offer some advantages. For instance, comparing cells with mutations in similar pathways (e.g., RAS versus PI3K, PTEN, and p53) could lead to more direct comparisons and a deeper understanding of circCD2AP expression in relation to these mutations. We will consider this aspect in our future studies.

STAR★METHODS

Detailed methods are provided in the online version of this paper and include the following:

- KEY RESOURCES TABLE

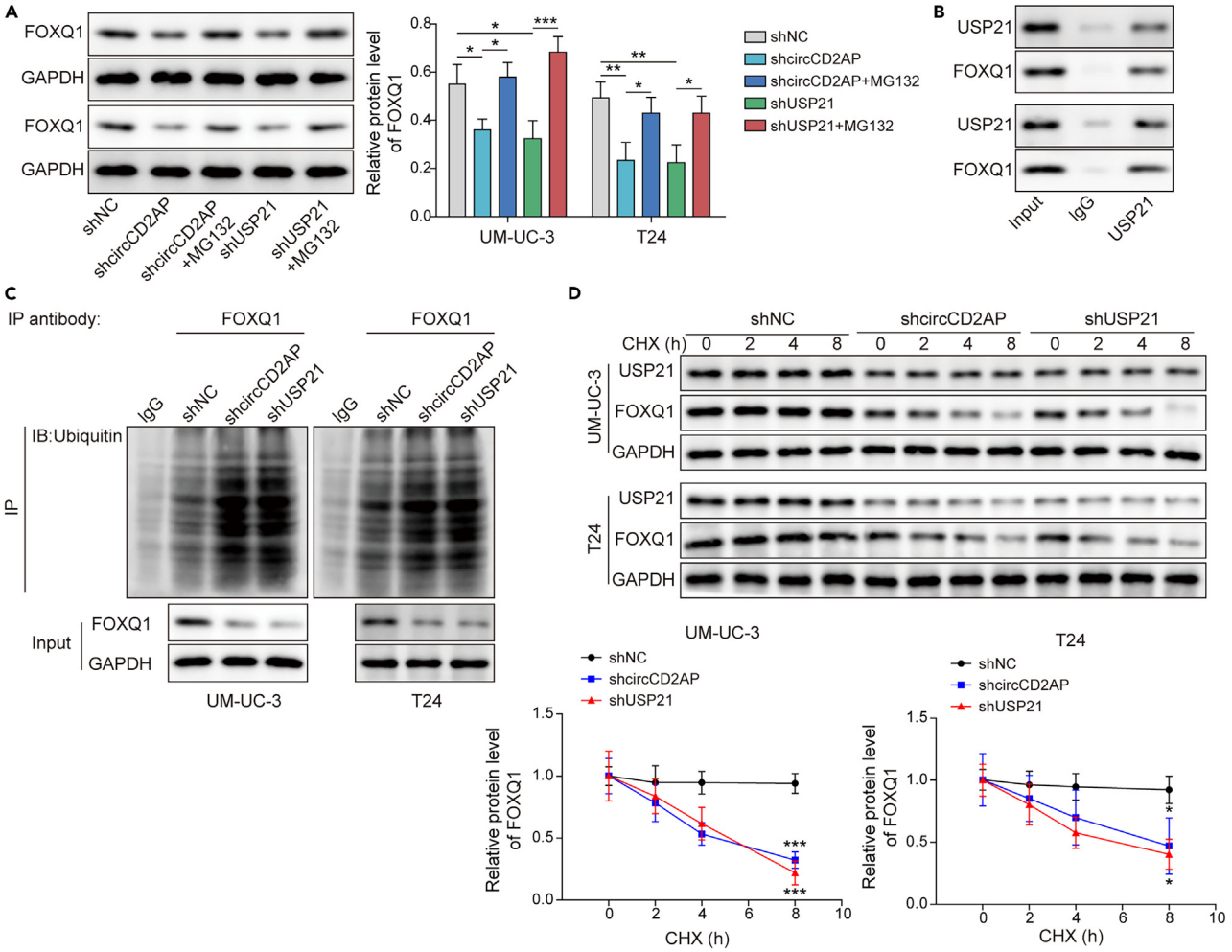

Figure 5. USP21 upregulated FOXQ1 by inhibiting its ubiquitination degradation

(A) Western blotting analysis of FOXQ1 in UM-UC-3 and T24 cells silenced circCD2AP or USP21 after treating with proteasome inhibitor MG132.

(B) The interaction between USP21 and FOXQ1 was analyzed by Co-IP.

(C) The ubiquitination levels of FOXQ1 were measured by Co-IP after silencing circCD2AP or USP21.

(D) After treating with CHX for indicated times (0, 2, 4, or 8 h), western blotting analyzed the degradation of FOXQ1 in UM-UC-3 and T24 cells transfected with shcircCD2AP or shUSP21. GAPDH used as control. Mean ± SD, n = 3, *p < 0.05, **p < 0.01, ***p < 0.001. Statistical analysis was carried out by a Student's t test or a one-way ANOVA.

- RESOURCE AVAILABILITY
  - Lead contact
  - Materials availability
  - Data and code availability
- EXPERIMENTAL MODEL AND STUDY PARTICIPANT DETAILS
- METHOD DETAILS
  - Cell transfection
  - Cytoplasm and nuclear fractionation
  - Fluorescence *in situ* hybridization (FISH)
  - Identification of circCD2AP
  - CCK-8 assay
  - Sphere-formation assay
  - Flow cytometric analysis of CD133
  - Wound healing assay
  - Analysis of the stability of USP21 mRNA

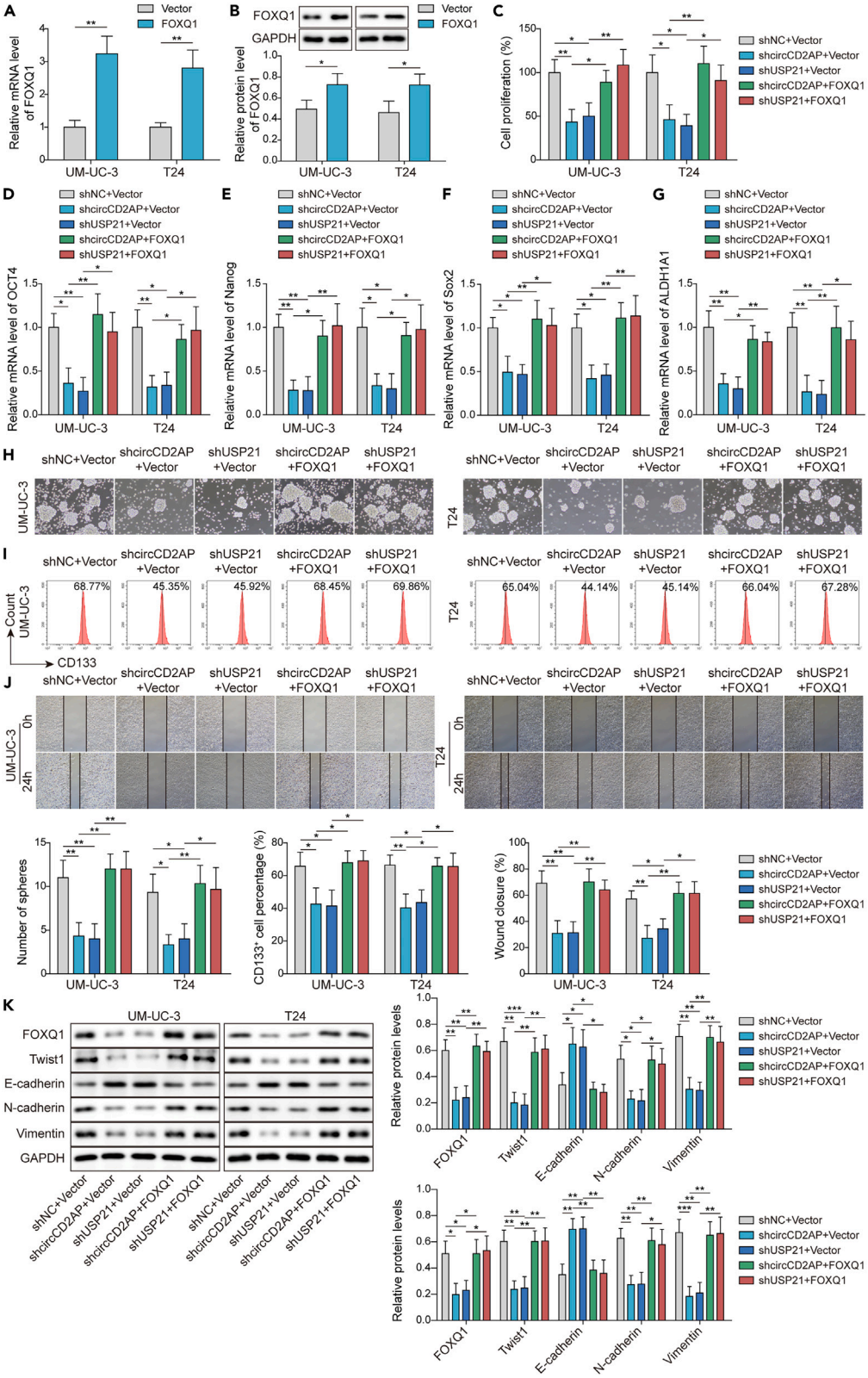
A
Vector
FOXQ1
Relative mRNA level of FOXQ1
UM-UC-3
T24
B
FOXQ1
GAPDH
Vector
FOXQ1
Relative protein level of FOXQ1
UM-UC-3
T24
C
Cell proliferation (%)
UM-UC-3
T24
shNC+Vector
shcircCD2AP+Vector
shUSP21+Vector
shcircCD2AP+FOXQ1
shUSP21+FOXQ1
D
Relative mRNA level of OCT4
E
Relative mRNA level of Nanog
F
Relative mRNA level of Sox2
G
Relative mRNA level of ALDH1A1
H
shNC+Vector
shcircCD2AP +Vector
shUSP21 +Vector
shcircCD2AP +FOXQ1
shUSP21 +FOXQ1
UM-UC-3
T24
I
Count
CD133
68.77%
45.35%
45.92%
68.45%
69.86%
65.04%
44.14%
45.14%
66.04%
67.28%
J
0h
24h
K
FOXQ1
Twist1
E-cadherin
N-cadherin
Vimentin
GAPDH
Relative protein levels
Number of spheres
CD133+ cell percentage (%)
Wound closure (%)

Figure 6. circCD2AP promoted EMT and stemness of BC cells through regulating USP21/FOXQ1 axis

(A and B) qRT-PCR and western blotting analysis of overexpression efficiency of FOXQ1 plasmid in UM-UC-3 and T24 cells. GAPDH used as control.

(C) The viability of cancer cells co-transfected with shcircCD2AP or shUSP21+FOXQ1 was assessed by CCK8.

(D–G) The expression of OCT4, Nanog, Sox2, and ALDH1A1 was evaluated by qRT-PCR after simultaneously silencing circCD2AP or USP21 and overexpressing FOXQ1.

(H) Cancer cell stemness was evaluated by sphere-formation assay after simultaneously silencing circCD2AP or USP21 and overexpressing FOXQ1.

(I) The percentage of $CD133^+$ cells was analyzed in cells co-transfected with shcircCD2AP or shUSP21+FOXQ1 by flow cytometry.

(J) The migration of cells co-transfected with shcircCD2AP or shUSP21+FOXQ1 was measured by wound-healing assay.

(K) Western blotting analysis of FOXQ1, Twist1, N-cadherin, E-cadherin, and vimentin after simultaneously silencing circCD2AP or USP21 and overexpressing FOXQ1. GAPDH used as a control. Mean ± SD, n = 3, *p < 0.05, **p < 0.01, ***p < 0.001. Statistical analysis was carried out by a one-way ANOVA.

SUPPLEMENTAL INFORMATION

Supplemental information can be found online at https://doi.org/10.1016/j.isci.2023.108447.

ACKNOWLEDGMENTS

Not applicable.

AUTHOR CONTRIBUTIONS

Jinrong Wang designed the experiments and wrote the manuscript. Jing Tan performed most of the experiments. Yichuan Zhang performed some of the experiments. Lei Zhou analyzed the data. Yuan Liu organized the figures. Jinrong Wang revised the article.

DECLARATION OF INTERESTS

The authors declare no competing interests.

Received: May 30, 2023
Revised: August 28, 2023
Accepted: November 10, 2023
Published: November 14, 2023

REFERENCES

1. Alfred Witjes, J., Lebret, T., Compérat, E.M., Cowan, N.C., De Santis, M., Bruins, H.M., Hernández, V., Espinós, E.L., Dunn, J., Rouanne, M., et al. (2017). Updated 2016 EAU Guidelines on Muscle-invasive and Metastatic Bladder Cancer. Eur. Urol. *71*, 462–475.
2. Chavan, S., Bray, F., Lortet-Tieulent, J., Goodman, M., and Jemal, A. (2014). International variations in bladder cancer incidence and mortality. Eur. Urol. *66*, 59–73.
3. Smith, N.D., Prasad, S.M., Patel, A.R., Weiner, A.B., Pariser, J.J., Razmaria, A., Maene, C., Schuble, T., Pierce, B., and Steinberg, G.D. (2016). Bladder Cancer Mortality in the United States: A Geographic and Temporal Analysis of Socioeconomic and Environmental Factors. J. Urol. *195*, 290–296.
4. Szabados, B., van Dijk, N., Tang, Y.Z., van der Heijden, M.S., Wimalasingham, A., Gomez de Liano, A., Chowdhury, S., Hughes, S., Rudman, S., Linch, M., and Powles, T. (2018). Response Rate to Chemotherapy After Immune Checkpoint Inhibition in Metastatic Urothelial Cancer. Eur. Urol. *73*, 149–152.
5. Kristensen, L.S., Andersen, M.S., Stagsted, L.V.W., Ebbesen, K.K., Hansen, T.B., and Kjems, J. (2019). The biogenesis, biology and characterization of circular RNAs. Nat. Rev. Genet. *20*, 675–691.
6. Chen, L., and Shan, G. (2021). CircRNA in cancer: Fundamental mechanism and clinical potential. Cancer Lett. *505*, 49–57.
7. Long, F., Lin, Z., Li, L., Ma, M., Lu, Z., Jing, L., Li, X., and Lin, C. (2021). Comprehensive landscape and future perspectives of circular RNAs in colorectal cancer. Mol. Cancer *20*, 26.
8. Qiu, F., Liu, Q., Xia, Y., Jin, H., Lin, Y., and Zhao, X. (2022). Circ_0000658 knockdown inhibits epithelial-mesenchymal transition in bladder cancer via miR-498-induced HMGA2 downregulation. J. Exp. Clin. Cancer Res. *41*, 22.
9. Fan, L., Yang, J., Shen, C., Wu, Z., and Hu, H. (2021). Circ_0030586 inhibits cell proliferation and stemness in bladder cancer by inactivating the ERK signaling via miR-665/NR4A3 axis. Acta Histochem. *123*, 151745.
10. Liu, L., Wu, S.Q., Zhu, X., Xu, R., Ai, K., Zhang, L., and Zhao, X.K. (2019). Analysis of ceRNA network identifies prognostic circRNA biomarkers in bladder cancer. Neoplasma *66*, 736–745.
11. Zhou, W.Y., Cai, Z.R., Liu, J., Wang, D.S., Ju, H.Q., and Xu, R.H. (2020). Circular RNA: metabolism, functions and interactions with proteins. Mol. Cancer *19*, 172.
12. Chen, R., Zhang, X., and Wang, C. (2020). LncRNA HOXB-AS1 promotes cell growth in multiple myeloma via FUT4 mRNA stability by ELAVL1. J. Cell. Biochem. *121*, 4043–4051.
13. Johnston, J.A., and Burrows, J.F. (2006). De-ubiquitinating enzymes: intracellular signalling and disease. Biochem. Soc. Trans. *34*, 764–769.
14. Liu, X., Yao, Y., Ding, H., Han, C., Chen, Y., Zhang, Y., Wang, C., Zhang, X., Zhang, Y., Zhai, Y., et al. (2016). USP21 deubiquitylates

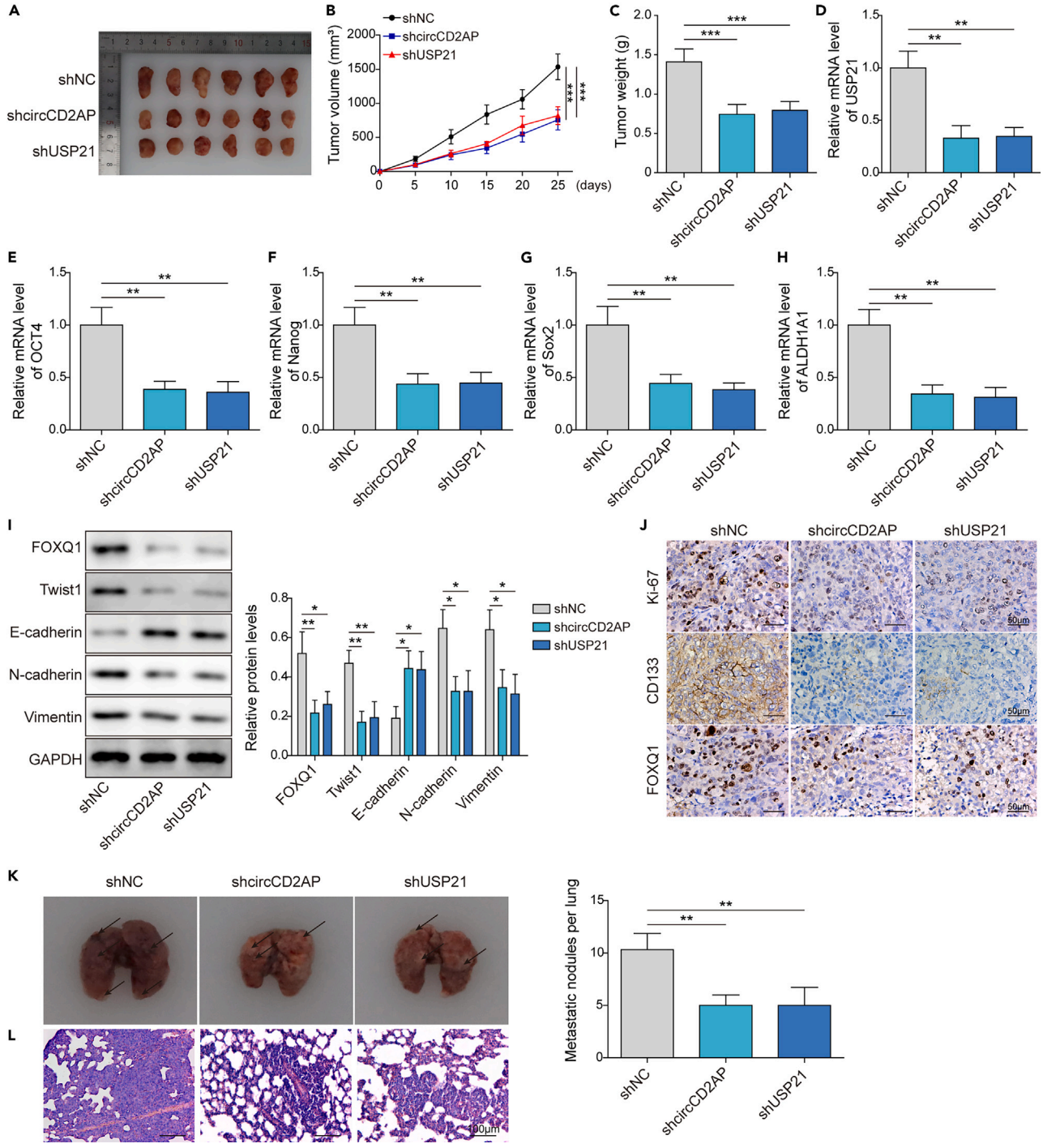

Figure 7. Knockdown of circCD2AP inhibited tumor formation and lung metastasis through suppression of USP21-mediated FOXQ1 signaling in nude mice

Nude mice were divided into three groups, and T24 cells that stably expressed shNC, shcircCD2AP, or shUSP21 were injected subcutaneously into the backs of mice (1×10^6 cells per mice) (n = 6). (A–C) Tumor images are shown, and the growth curves were calculated based on the average weight and volume of tumors in each group. (D–H) qRT-PCR analysis of USP21, OCT4, Nanog, Sox2, and ALDH1A1 in tumor tissues.

(I) Western blotting analysis of FOXQ1, Twist1, N-cadherin, E-cadherin, and vimentin. GAPDH used as control.

Figure 7. *Continued*

(J) Representative images of IHC staining showing expression of protein Ki-67, CD133, and FOXQ1 in tumor tissues of each group. Scale bar: 50 μm. To analyze lung metastasis, 1×10^6 shNC, shcircCD2AP, or shUSP21 stably infected T24 cell was injected into mouse tail veins (n = 6).

(K) Photograph of entire lungs from nude mice in each group.

(L) The number of lung metastatic nodules were counted by hematoxylin and eosin (HE) staining. Scale bar: 100 μm. Mean ± SD, *p < 0.05, **p < 0.01, ***p < 0.001. Statistical analysis was carried out by a one-way ANOVA.

Nanog to regulate protein stability and stem cell pluripotency. Signal Transduct. Target. Ther. *1*, 16024.

15. Chen, Y., Zhou, B., and Chen, D. (2017). USP21 promotes cell proliferation and metastasis through suppressing EZH2 ubiquitination in bladder carcinoma. OncoTargets Ther. *10*, 681–689.
16. Hou, P., Ma, X., Zhang, Q., Wu, C.J., Liao, W., Li, J., Wang, H., Zhao, J., Zhou, X., Guan, C., et al. (2019). USP21 deubiquitinase promotes pancreas cancer cell stemness via Wnt pathway activation. Genes Dev. *33*, 1361–1366.
17. Hannenhalli, S., and Kaestner, K.H. (2009). The evolution of Fox genes and their role in development and disease. Nat. Rev. Genet. *10*, 233–240.
18. Tan, J., Liu, B., Zhou, L., Gao, J., Wang, X.K., Liu, Y., and Wang, J.R. (2022). LncRNA TUG1 promotes bladder cancer malignant behaviors by regulating the miR-320a/FOXQ1 axis. Cell. Signal. *91*, 110216.
19. Han, S., Shi, Y., Sun, L., Liu, Z., Song, T., and Liu, Q. (2019). MiR-4319 induced an inhibition of epithelial-mesenchymal transition and prevented cancer stemness of HCC through targeting FOXQ1. Int. J. Biol. Sci. *15*, 2936–2947.
20. Zhu, Z., Zhu, Z., Pang, Z., Xing, Y., Wan, F., Lan, D., and Wang, H. (2013). Short hairpin RNA targeting FOXQ1 inhibits invasion and metastasis via the reversal of epithelial-mesenchymal transition in bladder cancer. Int. J. Oncol. *42*, 1271–1278.
21. Arceci, A., Bonacci, T., Wang, X., Stewart, K., Damrauer, J.S., Hoadley, K.A., and Emanuele, M.J. (2019). FOXM1 Deubiquitination by USP21 Regulates Cell Cycle Progression and Paclitaxel Sensitivity in Basal-like Breast Cancer. Cell Rep. *26*, 3076–3086.e6.
22. Tran, L., Xiao, J.F., Agarwal, N., Duex, J.E., and Theodorescu, D. (2021). Advances in bladder cancer biology and therapy. Nat. Rev. Cancer *21*, 104–121.
23. Alexandrov, L.B., Nik-Zainal, S., Wedge, D.C., Aparicio, S.A.J.R., Behjati, S., Biankin, A.V., Bignell, G.R., Bolli, N., Borg, A., Børresen-Dale, A.L., et al. (2013). Signatures of mutational processes in human cancer. Nature *500*, 415–421.
24. Cheung, G., Sahai, A., Billia, M., Dasgupta, P., and Khan, M.S. (2013). Recent advances in the diagnosis and treatment of bladder cancer. BMC Med. *11*, 13.
25. Meng, S., Zhou, H., Feng, Z., Xu, Z., Tang, Y., Li, P., and Wu, M. (2017). CircRNA: functions and properties of a novel potential biomarker for cancer. Mol. Cancer *16*, 94.
26. Lei, B., Tian, Z., Fan, W., and Ni, B. (2019). Circular RNA: a novel biomarker and therapeutic target for human cancers. Int. J. Med. Sci. *16*, 292–301.
27. Cai, Z., and Li, H. (2020). Circular RNAs and Bladder Cancer. OncoTargets Ther. *13*, 9573–9586.
28. Cheng, F., Zheng, B., Si, S., Wang, J., Zhao, G., Yao, Z., Niu, Z., and He, W. (2021). The Roles of CircRNAs in Bladder Cancer: Biomarkers, Tumorigenesis Drivers, and Therapeutic Targets. Front. Cell Dev. Biol. *9*, 666863.
29. Chen, L., Yang, X., Zhao, J., Xiong, M., Almaraihah, R., Chen, Z., and Hou, T. (2020). Circ_0008532 promotes bladder cancer progression by regulation of the miR-155-5p/miR-330-5p/MTGR1 axis. J. Exp. Clin. Cancer Res. *39*, 94.
30. Maraver, A., Fernandez-Marcos, P.J., Cash, T.P., Mendez-Pertuz, M., Dueñas, M., Maietta, P., Martinelli, P., Muñoz-Martin, M., Martínez-Fernández, M., Cañamero, M., et al. (2015). NOTCH pathway inactivation promotes bladder cancer progression. J. Clin. Invest. *125*, 824–830.
31. Chen, Q., Yin, Q., Mao, Y., Zhang, Z., Wu, S., Cheng, Z., Chen, X., Xu, H., Jin, S., Jiang, H., and Yang, C. (2020). Hsa_circ_0068307 mediates bladder cancer stem cell-like properties via miR-147/c-Myc axis regulation. Cancer Cell Int. *20*, 151.
32. Kristensen, L.S., Hansen, T.B., Venø, M.T., and Kjems, J. (2018). Circular RNAs in cancer: opportunities and challenges in the field. Oncogene *37*, 555–565.
33. Tan, S., Kang, Y., Li, H., He, H.Q., Zheng, L., Wu, S.Q., Ai, K., Zhang, L., Xu, R., Zhang, X.Z., et al. (2021). circST6GALNAC6 suppresses bladder cancer metastasis by sponging miR-200a-3p to modulate the STMN1/EMT axis. Cell Death Dis. *12*, 168.
34. Li, Y., Wan, B., Liu, L., Zhou, L., and Zeng, Q. (2019). Circular RNA circMTO1 suppresses bladder cancer metastasis by sponging miR-221 and inhibiting epithelial-to-mesenchymal transition. Biochem. Biophys. Res. Commun. *508*, 991–996.
35. Lu, Q., Liu, T., Feng, H., Yang, R., Zhao, X., Chen, W., Jiang, B., Qin, H., Guo, X., Liu, M., et al. (2019). Circular RNA circSLC8A1 acts as a sponge of miR-130b/miR-494 in suppressing bladder cancer progression via regulating PTEN. Mol. Cancer *18*, 111.
36. Mukherjee, N., Corcoran, D.L., Nusbaum, J.D., Reid, D.W., Georgiev, S., Hafner, M., Ascano, M., Jr., Tuschl, T., Ohler, U., and Keene, J.D. (2011). Integrative regulatory mapping indicates that the RNA-binding protein HuR couples pre-mRNA processing and mRNA stability. Mol. Cell *43*, 327–339.
37. Abdelmohsen, K., Panda, A.C., Munk, R., Grammatikakis, I., Dudekula, D.B., De, S., Kim, J., Noh, J.H., Kim, K.M., Martindale, J.L., and Gorospe, M. (2017). Identification of HuR target circular RNAs uncovers suppression of PABPN1 translation by CircPABPN1. RNA Biol. *14*, 361–369.
38. García-Santisteban, I., Bañuelos, S., and Rodríguez, J.A. (2012). A global survey of CRM1-dependent nuclear export sequences in the human deubiquitinase family. Biochem. J. *441*, 209–217.
39. Guo, Q., Shi, D., Lin, L., Li, H., Wei, Y., Li, B., and Wu, D. (2021). De-Ubiquitinating Enzymes USP21 Regulate MAPK1 Expression by Binding to Transcription Factor GATA3 to Regulate Tumor Growth and Cell Stemness of Gastric Cancer. Front. Cell Dev. Biol. *9*, 641981.
40. Fan, Y., Mao, R., Yu, Y., Liu, S., Shi, Z., Cheng, J., Zhang, H., An, L., Zhao, Y., Xu, X., et al. (2014). USP21 negatively regulates antiviral response by acting as a RIG-I deubiquitinase. J. Exp. Med. *211*, 313–328.
41. Zhang, J., Chen, C., Hou, X., Gao, Y., Lin, F., Yang, J., Gao, Z., Pan, L., Tao, L., Wen, C., et al. (2013). Identification of the E3 deubiquitinase ubiquitin-specific peptidase 21 (USP21) as a positive regulator of the transcription factor GATA3. J. Biol. Chem. *288*, 9373–9382.
42. Qiao, Y., Jiang, X., Lee, S.T., Karuturi, R.K.M., Hooi, S.C., and Yu, Q. (2011). FOXQ1 regulates epithelial-mesenchymal transition in human cancers. Cancer Res. *71*, 3076–3086.
43. Yang, M., Liu, Q., Dai, M., Peng, R., Li, X., Zuo, W., Gou, J., Zhou, F., Yu, S., Liu, H., and Huang, M. (2022). FOXQ1-mediated SIRT1 upregulation enhances stemness and radio-resistance of colorectal cancer cells and restores intestinal microbiota function by promoting beta-catenin nuclear translocation. J. Exp. Clin. Cancer Res. *41*, 70.
44. Zhang, X., Wang, L., Wang, Y., Shi, S., Zhu, H., Xiao, F., Yang, J., Yang, A., and Hao, X. (2016). Inhibition of FOXQ1 induces apoptosis and suppresses proliferation in prostate cancer cells by controlling BCL11A/MDM2 expression. Oncol. Rep. *36*, 2349–2356.
45. Yang, J., Qi, M., Fei, X., Wang, X., and Wang, K. (2022). Hsa_circRNA_0088036 acts as a ceRNA to promote bladder cancer progression by sponging miR-140-3p. Cell Death Dis. *13*, 322.
46. Hong, X., Liu, N., Liang, Y., He, Q., Yang, X., Lei, Y., Zhang, P., Zhao, Y., He, S., Wang, Y., et al. (2020). Circular RNA CRIM1 functions as a ceRNA to promote nasopharyngeal carcinoma metastasis and docetaxel chemoresistance through upregulating FOXQ1. Mol. Cancer *19*, 33.

STAR★METHODS

KEY RESOURCES TABLE

REAGENT or RESOURCE	SOURCE	IDENTIFIER
Antibodies		
Mouse monoclonal anti-CD133	ThermoFisher	Cat# 12-1338-42; RRID:AB_1582257
Rabbit monoclonal anti-ELAVL1	Abcam	Cat# ab200342; RRID:AB_2784506
Rabbit monoclonal anti-USP21	ThermoFisher	Cat# 17856-1-AP; RRID:AB_2878453
Mouse monoclonal anti-FOXQ1	Santa Cruz Biotechnology	Cat# sc-166265; RRID:AB_2105178
Anti-IgG	Abcam	Cat# ab6789; RRID:AB_955439
Rabbit monoclonal anti- ubiquitin	Abcam	Cat# ab140601; RRID:AB_2783797
Rabbit monoclonal anti-Ki-67	Abcam	Cat# ab16667; RRID:AB_302459
Mouse monoclonal anti-FOXQ1	ThermoFisher	Cat# PA5-98924; RRID:AB_2813537
Rabbit recombinant multiclonal anti-CD133	Abcam	Cat# ab284389; RRID:AB_2939000
Horseradish peroxidase-conjugated goat anti-rabbit antibody	Santa Cruz Biotechnology	Cat# sc-2004; RRID:AB_631746
Mouse monoclonal anti-Twist1	Abcam	Cat# ab50887; RRID:AB_883294
Rabbit monoclonal anti-E-cadherin	Abcam	Cat# ab76319; RRID:AB_2076796
Rabbit monoclonal anti-N-cadherin	Abcam	Cat# ab76011; RRID:AB_1310479
Rabbit monoclonal anti-Vimentin	Abcam	Cat# ab92547; RRID:AB_10562134
Chemicals		
Actinomycin D	ThermoFisher	Cat# 11805-017
MG132	Sigma	Cat# M7449
cycloheximide	Sigma	Cat# C7698
Critical commercial assays		
Ambion® PARIS™ Kits	Invitrogen	Cat# AM1921
Cell Counting Kit-8 reagent	Beyotime	Cat# C0038
Magnetic RNA-protein Pull-down Kit	ThermoFisher	Cat# 20164
Trizol reagent	Invitrogen	Cat# 15596026
SYBR™ Green PCR Master Mix	ThermoFisher	Cat# 4309155
Experimental models: Cell lines and mice		
BC cell lines (5637, T24, UM-UC-3, BT-B, and J82)	American Type Culture Collection	N/A
SV-HUC-1 cells	Procell Life Science&Technology Co.,Ltd.	N/A
BABL/c nude mice	human SJA laboratory animal co., LTD	N/A
Oligonucleotides		
shcircCD2AP	GenePharma	N/A
shUSP21	GenePharma	N/A
shFOXQ1	GenePharma	N/A
shELAVL1	GenePharma	N/A
shcircCD2AP1#2-Res	GenePharma	N/A
qRT-PCR primer sequences please see Table S1	This paper	N/A
Software and algorithms		
GraphPad Prism 8.0	GraphPad	https://www.graphpad.com/scientificsoftware/prism/
UALCAN database		https://ualcan.path.uab.edu/analysis.html/

RESOURCE AVAILABILITY

Lead contact

Further information and requests for resources and reagents should be directed to and will be fulfilled by the lead contact, Jinrong Wang (xy3yywjr@163.com).

Materials availability

This study did not generate any unique new reagent. All reagents used in this study are commercially available.

Data and code availability

All data reported in this paper will be shared by the lead contact upon request.

These paper does not report original code.

Any additional information required to reanalyze the data reported in this paper is available from the lead upon request.

All authors have approved the experiments and all experiments conform to the relevant regulatory standards.

EXPERIMENTAL MODEL AND STUDY PARTICIPANT DETAILS

52 individuals with BC who had received radical cystectomy at the Third Xiangya Hospital of Central South University were included. The clinicopathological characteristics of these BC patients (East Asian population) were listed in Table 1. Collected cancer tissue and pair-matched adjacent healthy tissue were divided into equal size and frozen in liquid nitrogen. Informed consent was obtained from all participants. The Ethics Committee of the Third Xiangya Hospital of Central South University approved this study (No: 2017-S254).

BC cell lines (5637, T24, UM-UC-3, BT-B, and J82) were obtained from American Type Culture Collection (Manassas, VA, USA) and human normal bladder epithelial cells (SV-HUC-1) were obtained from Procell Life Science&Technology Co.,Ltd. (Wuhan, China). SV-HUC-1 cells were cultured in F12K medium, BT-B and 5637 cells were cultured in RPMI-1640 medium, and other cells were cultured in DMEM medium at 37°C supplied with 5% CO_2. All these mediums contained 10% FBS, 100 μg/mL streptomycin, and 100 U/mL ampicillin (all from Gibco, Carlsbad, USA).

Mouse-related experiments were approved by the Animal Care and Use Committee of Third Xiangya Hospital of Central South University (No: LLSC(LA)2017-039). BABL/c nude mice (6 weeks, 16-20g) purchased from human SJA laboratory animal co., LTD (Hunan, China) under specific pathogen-free circumstances (20°C; 60% humidity and alternate 12-h light/dark cycles), free access to food and water.

METHOD DETAILS

Cell transfection

The full length of circCD2AP, USP21, FOXQ1 coding sequence was amplified and cloned into a pcDNA3.1 (Invitrogen, Carlsbad, CA, USA) vector (circCD2AP, USP21, FOXQ1). Short hairpin RNA (shRNA) targeted circCD2AP, USP21, FOXQ1, ELAVL1 (shcircCD2AP, shUSP21, shFOXQ1, shELAVL1) or scrambled oligonucleotides (all provided by Shanghai GenePharma) were inserted into pGLVH1 vector. shRNA-resistant circCD2AP (shcircCD2AP1#2-Res) was also designed and provided by GeneParma. Lipofectamine 3000 transfection reagent (Invitrogen) used for all plasmids transfection. Lenti-Pac HIV Expression Packaging Mix and the lentiviral vectors (shcircCD2AP, shUSP21) were used to transfect HEK293T cells for 48 h and then lentiviral particles were harvested from the supernatant. Stable transfected cells were selected by two weeks puromycin treatment (2 μg/mL).

Cytoplasm and nuclear fractionation

The Ambion PARIS Kits (Invitrogen) were performed for subcellular fractions. Briefly, after resuspending in the fraction buffer and incubating on ice, collected cells were centrifuged with supernatant discarded. Following that, extracted nuclear and cytoplasmic RNA was analyzed by subsequent qRT-PCR.

Fluorescence *in situ* hybridization (FISH)

Cy3-labled circCD2AP probes were designed and supplied by Genema (Shanghai, China). Cells were seeded on coverslips and allowed to growth for 24 h, followed by the fixation with 4% paraformaldehyde. Next, cells were incubated with the circCD2AP probe (1: 50) overnight. Finally, signals in nucleus were observed after DAPI staining using a confocal microscope (Olympus, Tokyo, Japan).

Identification of circCD2AP

The circCD2AP sequence obtained using divergent primers was sent to Sangon (Shanghai, China) for Sanger sequencing analysis. Actinomycin D (act-D) and RNase R treatment evaluated circCD2AP stability through qRT-PCR. Cells were incubated with 5 μg/mL act-D in DMEM medium for 0, 4, 8, 12, and 24 h. Cells were harvested at the indicated time. RNA was extracted and cultured with RNase R (20 U/μL) at 37°C for 1 h.

CCK-8 assay

Cells (1×10^5/mL) were seeded in 96-well plates and cultured overnight. 10 μL of the Cell Counting Kit-8 (CCK-8) reagent (Beyotime, China) was added to each well, and cells were incubated for 4 h at 37°C. The absorbance of transfected cells was detected at 450 nm by a spectrophotometer (BioRad, Hercules, CA, USA).

Sphere-formation assay

Single-cell suspension cultures were prepared in serum-free DMEM/F12 (Gibco) medium supplement with a combination of insulin, 20 ng/mL human recombinant epidermal growth factor (EGF; Gibco), and 10 ng/mL basic fibroblastic growth factor (FGF; Invitrogen), and then seeded into 6-well ultra-low attachment plates. After 2 weeks, spheroids clones were stained with crystal violet and counted under a light stereomicroscope (Olympus).

Flow cytometric analysis of CD133

After trypsinizing, suspending in PBS and fixing with 4% formaldehyde, cells were stained with CD133-FITC antibody (12-1338-42; ThermoFisher, Waltham, MA, USA) for 30 min in the dark. Stained cells were then analyzed by FACS Calibur (BD Biosciences, San Jose, CA, USA) and the percentage of $CD133^+$ stem cells was quantified.

Wound healing assay

After culturing to 90–95% confluence, cells were wounded by a plastic spatula in 6-well plates. Afterward, cells were washed with PBS twice to remove the cell debris and cultured in an FBS free medium for 24 h. The healing was then observed via a light microscope.

Analysis of the stability of USP21 mRNA

Cells silenced circCD2AP or ELAVL1 were incubated with act-D (5 μg/mL) and then harvested. Following that, RNA was isolated immediately (t = 0) or at indicated time (t = 4, 8, 12) after adding act-D. The stability was evaluated via qRT-PCR.

RNA pull-down

Magnetic RNA-protein Pull-down Kit (ThermoFisher) was used to conduct circCD2AP pulldown. Biotinylated DNA probe targeting back-splicing sequence of circCD2AP was designed for capturing circCD2AP from total RNA. Briefly, isolated total RNA was incubated with 100 nmol DNA probe, and then bound to 50 μL Streptavidin Magnetic Beads lysates. Next, lysate was incubated for 2 h at 4°C with rotation in 100 μL × RNA-protein binding buffer containing 100 μg total protein. After washing, complexes were isolated from streptavidin Magnetic Beads. ELAVL1 was assessed in the pulldown by Western blotting.

RNA immunoprecipitation (RIP)

After cross-linking with formaldehyde, cells were harvested. Then, cells were resuspended in RIP buffer, supplemented with protease and RNase inhibitors, followed by incubating with magnetic beads conjugated with anti-ELAVL1 (ab200342, Abcam, Cambridge, UK) or IgG overnight with rotation. RNA was eluted in RIP elution buffer and then extracted and enriched.

Co-immunoprecipitation

Cells were lysed in lysis buffer and centrifuged at 12000g to obtain supernatant, with a fraction pipetted out as Input. After adding the IP buffer, anti-USP21 (17856-1-AP, ThermoFisher), anti-FOXQ1 (sc-166265, Santa Cruz Biotechnology) or IgG (ab6789, Abcam) antibody was added to sample and incubated overnight. Immune complexes were isolated by protein A/G beads. Coimmunoprecipitates were resolved by SDS-PAGE and measured using anti-FOXQ1 or anti-ubiquitin (ab140601, Abcam) antibodies via Western blotting.

Animal experiments

Male nude mice were injected with T24 cells (1×10^6) stably expressed shNC, shcircCD2AP, or shUSP21 through subcutaneous injection (n = 6). Tumor volumes were recorded every 5 days. After 25 days, tumor tissues were collected from mice (intraperitoneal injected with sodium pentobarbital (120 mg/kg) to put them to euthanasia) for subsequent experiments.

For metastasis models, 1×10^6 shNC, shcircCD2AP, or shUSP21 stably infected T24 cell was injected into mouse tail veins (n = 6). After 25 days, lung tissues were isolated for analyzing lung metastasis. First, tissues images were captured. Tissues were then made into 5 μm sections, followed by dewaxing and dehydrating. Slices were subsequently stained with Hematoxylin and eosin (H&E) and imaged using a microscope (Olympus).

Immunohistochemistry (IHC)

Slices of tissues were subjected to antigen retrieval by heating in a microwave oven in 10 mmol/L citrate buffer for 3 min. Then, sections were incubated with primary antibodies against Ki-67 (ab16667, Abcam), FOXQ1 (MA5-17078, ThermoFisher) and CD133 (ab284389, Abcam) at 4°C

overnight. Afterward, slices were incubated with poly-peroxidase-*anti*-mouse/rabbit IgG and detected using DAB (Bioss, Beijing, China). Hematoxylin-based reagents were used to create the immunohistochemistry response, which was subsequently seen under a microscope.

Quantitative real-time PCR (qRT-PCR)

Total RNAs were extracted with Trizol reagent (Invitrogen) and reverse-transcribed to cDNA with Prime-Script RT-PCR master mix (Takara, Tokyo, Japan). RT-qPCR detection of circCD2AP, OCT4, Nanog, Sox2, ALDH1A1, CD44v6, USP21, and FOXQ1 mRNA expression levels was performed with SYBR Green qPCR (4309155, ThermoFisher). GAPDH regarded as a control and gene expression was presented as fold changes relative to the expression of appropriate controls using the $2^{-\Delta\Delta Ct}$ method. The primer sequences were shown Table S1.

Western blot analysis

Proteins were extracted from cells and tissues, and the concentration was quantified by BCA kits. Typical SDS (10%)-polyacrylamide gels was utilized to purify the proteins (~30 μg) extracted from every group. Afterward, the purified proteins were transferred to a polyvinylidene difluoride (PVDF) membrane. Placed the membrane into a Petri dish containing 5% milk for 1 h to block non-specific sites. Discarded the milk and rinse the membranes and dish three times with PBS, then added the PBS containing primary antibodies into the dish. After overnight incubation, rinse the membrane and dish again three times with PBS, then added horseradish peroxidase-conjugated secondary antibody (sc 2004, Santa Cruz Biotechnology) and incubated for 1 h. The antibody-reactive bands were detected with ECL reagent (Millipore, Billerica, MA, USA). GAPDH (ab8245, Abcam) regarded as a control. Primary antibodies showed as below: anti-FOXQ1 (MA5-17078, ThermoFisher), anti-Twist1 (ab50887, Abcam), anti-E-cadherin (ab76319, Abcam), anti-N-cadherin (ab76011, Abcam), anti-Vimentin (ab92547, Abcam), and anti-USP21 (17856-1-AP, ThermoFisher).

QUANTIFICATION AND STATISTICAL ANALYSIS

Data are expressed as the mean ± SD. GraphPad Prism 8.0 was used for statistical analysis. Differences in the overall survival (OS) were estimated and compared by the Kaplan–Meier method. Student's *t* test was performed to evaluate the differences between two groups; one-way ANOVA was performed to determine significant differences between multiple groups. p value lower than 0.05 ($p < 0.05$) was considered as statistically significant.